Hindawi
Advances in Civil Engineering
Volume 2020, Article ID 8818949, 14 pages
https://doi.org/10.1155/2020/8818949

Research Article

Effect of Subway Excavation with Different Support Pressures on Existing Utility Tunnel in Xi'an Loess

Min Yang, Hongru Li, Ning Li, and Shun Yang

Institute of Geotechnical Engineering, Xi'an University of Technology, Xi'an, China

Correspondence should be addressed to Hongru Li; lhrbj@xaut.edu.cn

Received 2 June 2020; Revised 27 July 2020; Accepted 8 September 2020; Published 21 September 2020

Academic Editor: Tayfun Dede

The interaction between two shield tunnels and the integrated pipe corridor is complicated and still lacks understanding. This paper investigated the influence of the double-track subway construction on the deformation characteristics of the existing comprehensive pipe corridor based on numerical simulation on a case history in Xi'an, China. First, loess is a special kind of clayed soil. In the theoretical calculation of overburden earth pressure of shield tunnel, the loose earth pressure theory under the incomplete soil arching effect can be used for calculation when considering the soil arching effect. Then, in the loess area of Xi'an, the existing comprehensive pipe corridor is affected by the construction disturbance. The vertical displacement of the existing pipe corridor utility tunnel affected by different support pressures which considers the soil arch effect or not was extracted from the FEM. The results indicated that, in the case where the left and right lines are constructed at different times, the vertical displacement of the pipe gallery is affected by different support pressures. If the support pressure is small, the settlement will be large, and the uplift will be diminutive. According to the construction methods and supporting pressures of this article, shield tunnel construction will not damage the safety of the comprehensive pipe corridor.

1. Introduction

In urban areas, a utility tunnel is a kind of underground structure to transport water, sewage, oil, natural gas, and other materials. Utility tunnels have been widely constructed throughout the world after the first one was constructed in Paris in 1851. Nowadays, the domestic and foreign countries are in the period of high-speed development of underground space. The increasingly dense subway lines, pipelines, underground lane lines, and so on will restrict each other [1–3]. How to reduce the influence between the lines will be a big problem to be solved urgently in the construction of underground buildings in the future.

Therefore, it is encountered under the existing comprehensive pipe corridor in the process of using the shield method in the construction of subway tunnels. In addition, shield tunneling is often carried out in soft soil. Once the soil is disturbed, it is particularly easy to cause surface settlement and deformation of surrounding soil layers and upper pipelines [4–6]. This will greatly affect the stability of the existing comprehensive pipe gallery.

At present, amount of work has been carried out at home and abroad on the simulation research of the three-dimensional dynamic construction process of shield tunnels. A large number of studies have been conducted to investigate the impact of undercrossing shield tunneling on the existing tunnels [7–11]. And shield construction affects the internal force and deformation of adjacent buildings [12, 13].

However, the numerical simulation of the influence of shield tunnel three-dimensional dynamic construction process on the comprehensive pipe gallery is relatively rare. An increasing number of studies have been conducted on tunnel-pipe interaction, most of which chose to simplify tunnel-pipe interaction as a two-dimensional problem. These include several analytical solutions [14–18]. Wang et al. [19] developed a Winkler-based pipe-soil-tunneling interaction model, which is focused on different pipe-soil interactions in relative uplift and downward pipe movements. In Lin et al.'s study [20], analytical solutions

incorporating the tensionless Pasternak model, which takes full account of the gap formation and the pipeline orientation, have been formulated to estimate the response of the pipeline and the overlying ground. Since all these previous studies reduced the interaction of the tunnel and the pipeline to a two-dimensional problem, these three problems cannot be determined.

Therefore, it is particularly important to use numerical methods to simulate the impact of shield tunnel construction on the comprehensive pipe corridor, and the construction of the comprehensive pipe corridor has a long-term development plan in China. Based on the Xi'an subway shield tunnel passing through the existing comprehensive pipe corridor, this article will establish a numerical model to simulate the construction process of the subway shield tunnel passing through the existing comprehensive pipe corridor. The construction method of "line re-excavation" analyzes the influence of the shield tunneling on the deformation of the existing comprehensive pipe corridor under the conditions of considering the soil arch effect and the supporting pressure without considering the soil arch effect.

2. Related Theory of Shield Support Pressure

2.1. Theory of Terzaghi Loose Soil Pressure. Based on the assumption that the sliding surface is vertical, Terzaghi deduced that the loose earth pressure formula is widely used [21]:

$$\sigma_v = \frac{\gamma B - c}{K\tan\varphi}\left(1 - e^{((-KH\tan\varphi)/B)}\right) + qe^{((-KH\tan\varphi)/B)}, \quad B = R\cot\left(\frac{\pi}{8} + \frac{\varphi}{4}\right), \tag{1}$$

where K is the pressure coefficient of the soil side, the value is between 1.0 and 1.5, it is recommended to take 1.0; H is the height of the overlying soil; q is the upper load; R is the tunnel radius; B is the span of the cavern; φ is internal friction angle of soil; c is cohesion of soil; and γ is unit weight.

2.2. Loose Earth Pressure Theory under the Incomplete Soil Arching Effect. In the Terzaghi loose earth pressure theory, the selection of the lateral pressure coefficient of the soil is recommended to be 1.0. The selection of this value being the best one is arguable. Handy [22] analyzed the insufficiency of the pressure arch model and derived the coefficient of confinement pressure of the soil based on Mohr's circle of stress.

Since the shield driving method can better control the formation damage, it can be considered that the soil arching effect is not as assumed in the Terzaghi loose earth pressure. That is, the soil arch is an incomplete soil arch, and the arching effect is not fully exerted. Based on Handy's theory, Li [23] puts out the side compression of soil, considering the incomplete arch effect. Sketch of partially developed soil arching effect is shown in Figure 1.

Calculation formula for loose earth pressure under incomplete soil arching effect is as follows:

$$\sigma_v = \frac{B_1\gamma}{A_1}\left(1 - e^{(-A_1h/B_1)}\right) + qe^{(-A_1h/B_1)}, \tag{2}$$

$$A_1 = \frac{K(1 - K_a)\tan\theta}{1 + K_a\tan^2\theta}, \tag{3}$$

$$K = \frac{1 + K_a\tan^2\theta}{\tan^2\theta + K_a}. \tag{4}$$

For clayed soil, the active earth pressure coefficient should take cohesion into account in the soil lateral pressure coefficient formula. According to Rankine earth pressure theory, the active earth pressure coefficient K_a of clayed soil is

$$K_a = \tan^2\left(45^\circ - \frac{\varphi}{2}\right) - \frac{2c}{\gamma h}\tan\left(45^\circ - \frac{\varphi}{2}\right). \tag{5}$$

Therefore, when calculating the loosening earth pressure under the incomplete soil arch effect of cohesive soil, formula (6) can be substituted into formula (4) and formula (5) for calculation. It obtains the calculation formula of loose earth pressure under the incomplete soil arch effect considering cohesion as follows:

$$\sigma_v = \frac{B_1\gamma - c}{A_1}\left(1 - e^{(-A_1h/B_1)}\right) + qe^{(-A_1h/B_1)}. \tag{6}$$

In a certain case of K_a, A_1 and K are determined by θ, the greater the rate of ground loss, the larger the deflection angle of the maximum principal stress, resulting in the smaller the θ. Therefore, θ depends on the formation loss rate, and B_1 is the width of loose band. That is, displacement of the vault is

$$\tan\theta = \frac{B_1}{2s} - \frac{s}{2B_1}, \tag{7}$$

where s is the formation loss parameter, that is, the displacement of the arch surface of the excavation face.

2.3. Comparative Analysis of Earth Pressure at Tunnel Top. In the theory of loose earth pressure under the incomplete soil arching effect considering cohesion, the formation loss parameter is required. This parameter can be calculated by the equivalent formation loss formula proposed by Loganathan and Poulos [24]:

$$\varepsilon_0 = \frac{4sR + s^2}{4R^2} \times 100\%, \tag{8}$$

where ε_0 is the formation loss rate, R is the tunnel radius, and s is the gap parameter, which is also the vault sedimentation.

According to formula (8) transformation,

$$s = 2R\left(\sqrt{1 + \varepsilon_0} - 1\right). \tag{9}$$

Therefore, combined with the corresponding parameters, different loose soil pressure values can be calculated

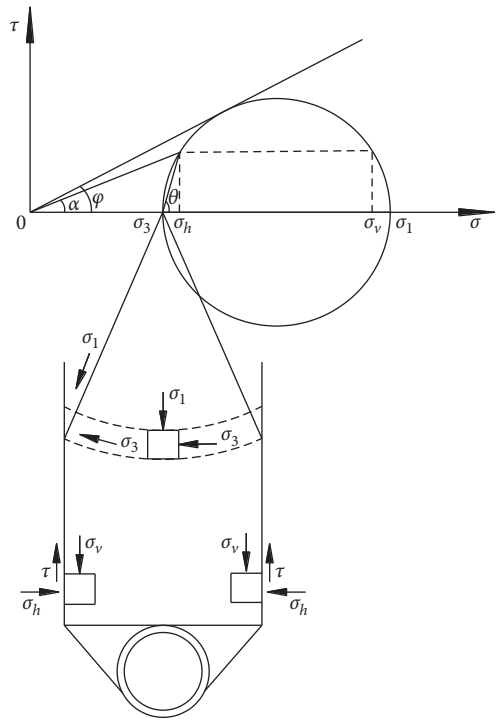

Figure 1: Sketch of partially developed soil arching effect.

Table 1: Soil basic physical property index.

Soil layer	γ (kN/m^3)	c (kPa)	φ (°)	Layer (m)
Soil 1	17	25	17	3
Soil 2	18.3	35	20	4
Soil 3	18.9	50	18	3
Soil 4	20.1	45	20	20

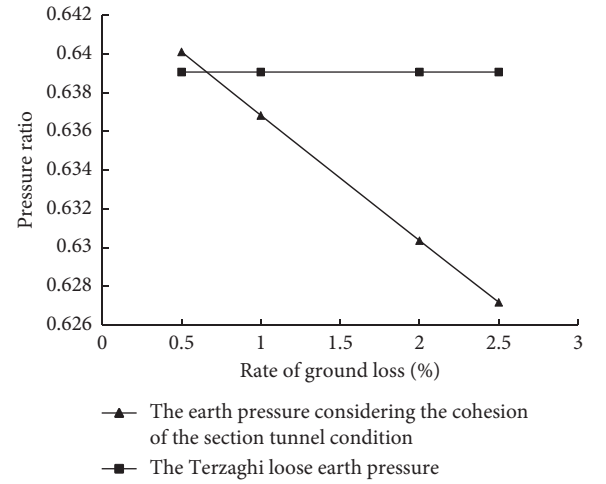

Figure 2: The pressure ratio in different strata loss rate.

under the incomplete soil arching effect considering cohesion.

The stratum parameters of a section of Xi'an Metro are shown in Table 1. The overlying soil thickness of the tunnel is 18.0, and the tunnel radius is 3.07.

According to the empirical data, the literature [25] concluded that the formation loss rate of the clay formation is about 0.5%~2.5%. By formula (6), the corresponding loose soil pressure value can be obtained under the incomplete soil arching effect considering the cohesion. Here, for the sake of convenience, the pressure ratio concept is applied in this paper. The pressure ratio is the ratio of the loose earth pressure σ_i to the full earth pressure σ_v at the soil:

$$\eta = \frac{\sigma_i}{\sigma_v}. \tag{10}$$

The pressure ratio of the earth pressure considering the cohesion of the section tunnel condition (η_p) is compared with the pressure ratio of the Terzaghi loose earth pressure (η_T), as shown in Figure 2.

Figure 2 shows that the law of different earth pressures can be obtained.

(1) Because the theory of loose earth pressure under the incomplete soil arching effect considering cohesion takes into account the rate of ground loss, there is a corresponding earth pressure value for different ground loss ratios. However, the ground loss ratio is not considered in the calculation of full overburden pressure and Terzaghi loose earth pressure, and the calculated earth pressure value is constant at a fixed depth and the hole diameter;

(2) Due to the soil arch effect, the theory of loose earth pressure under the incomplete soil arching effect considering cohesion and Terzaghi earth pressure are smaller than the full earth pressure. When the ground loss ratio is less, the earth pressure is not less different in value.

(3) When the ground loss ratio is less than 0.65%, the theory of loose earth pressure under the incomplete soil arching effect considering cohesion is larger than the Terzaghi earth pressure due to the less principal stress deflection angle. In the case where the ground loss ratio is greater than 0.65%, the soil arch effect is more obvious as the formation loss rate is larger, and the value of the theory of loose earth pressure under the incomplete soil arching effect considering cohesion is gradually reduced. Terzaghi earth pressure has not considered the formation loss, so the soil arching effect has always been a fixed value. That shows the rationality of the earth pressure method proposed by the author. That is, the greater the loss of the formation, the more obvious the soil arching effect.

3. Project Overview

The project studied herein is located in Metro Line 2 (ML2, in operation) in Xi'an City, China. ML2 consisted of twin single tube tunnels constructed by using the shield-driven method. The support method is prefabricated C50 reinforced concrete segments, which are connected by using bent bolts. The outer diameter of segments is 6.0 m, the ring

width is 1.5 m, and the thickness is generally 300 mm. The buried depth of the tunnel is generally between 8.0 m and 25.0 m, and the tunnel spacing is generally between 9 m and 20 m, except for the key protection of ancient buildings around the construction section.

In this paper, combined with a comprehensive pipe gallery project in Xi'an City, the subway tunnel is planned to be built under the comprehensive pipe gallery. The subway axis is parallel to the pipe gallery axis. The relative position of a cross section tunnel and the pipe gallery is shown in Figure 3.

The cross section of the comprehensive pipe gallery project is in the form of three tanks, including natural gas tank, comprehensive tank, and power tank. The buried depth of the pipe gallery is 3 m. The pipe gallery structure is made of C35 concrete, and its specific dimensions are shown in Figure 4.

Considering the economy, the construction method of the utility tunnel adopts the cut-and-cover method. The reinforcement form adopts sloping and soil nailing wall. The slope is 1 : 0.75. The excavation method adopts layered excavation. The excavation depth of each layer does not exceed 1.5 m and 2.0 m. After the excavation, shotcrete with mesh of C20 concrete is applied in time and then soil nails are applied. The soil nails are made of HRB400 steel bars with a diameter of 14 mm, a vertical spacing of 1.5 m, and a vertical spacing of 1.0 m. The thickness of sprayed concrete is 60 mm. When the excavation is 30 cm from the bottom of the pit, manual excavation shall be adopted. The bedding construction shall be completed within 24 hours of bottoming to minimize the exposure time of the soil at the bottom of the pit. The cushion thickness of 1.0 m shall be poured with C15 concrete. Since the left and right support and treatment of the utility tunnel are the same, only the right half of the utility tunnel is shown in Figure 5.

4. Three-Dimensional Numerical Model

4.1. Numerical Scheme. Since the theory of loose earth pressure under the incomplete soil arching effect considering cohesion is improved on the basis of Terzaghi's theory on loosening earth pressure, it is used as the calculation basis for considering the soil arch effect.

The supporting pressure is calculated by using the standard method [26]. The overburden pressure (σ_v) is calculated by the all-covering theory (without soil arch) and the theory of loose earth pressure under the incomplete soil arching effect considering cohesion (with soil arch). The distribution of support pressure is trapezoidal in Figure 6.

The supporting pressure on the edge of the tunnel is

$$\sigma_T = k\sigma_v + p_0. \tag{11}$$

The supporting pressure at the lower edge of the tunnel is

$$\sigma_T = k\left(\sigma_v + D\gamma\right) + p_0. \tag{12}$$

where k is the experienced coefficient, and in this article, 0.72 is taken as the value of k, the average from 0.65 to 0.85 [27]. p_0 is the preloading, generally 20~30kPa, and in this paper, 20 kPa is taken as the value of p_0. D is the diameter. γ is the soil volume weight behind heading face. σ_v is the overburden soil pressure of the tunnel.

The overburden pressure is carried out according to different calculation theories. The soil pressure of the theory of loose earth pressure under the incomplete soil arching effect considering cohesion is calculated according to the rate of ground loss of 0.5%. The calculation results are shown in Table 2.

In this paper, synchronous injection of inert grouting pressure simplifies the form of a uniform distribution of the entire ring. The tunnel radial outward uniform load is applied to the contact surface of the surrounding rock and the grouting layer, and the radial surface is applied to the outer surface of the segment, as shown in Figure 7.

This paper selects the optimal grouting pressure method. At the same time, the safety factor only considers the active earth pressure and the passive earth pressures [28]. The calculated optimal grouting pressure is 332.069 kPa.

4.2. FEM. A three-dimensional finite element model, using the commercial software Abaqus and Hyperworks, was established to investigate the utility tunnels deformation due to the construction of twin shield tunnels underneath. Figure 8 shows the finite element mesh used in this study, which was 120 m in length, 90 m in width, and 50 m in depth. Figure 9 gives details on the simulation of utility tunnels over new tunnels. Tunnel depth is 18 m. Tunnel clear distance is 18 m. The shield tunneling diameter is 6.14 m. Tunnel segment thickness is 0.3 m. The outer diameter of tunnel segment is 6.0 m.

According to the actual geological conditions of Xi'an in China, the soil layer is divided into 5 layers, the backfilling soil layer of pipe gallery is ①, and the stratum is ②~⑤ from top to bottom.

The soil layer, backfill, and cushion are made of C3D8 solid element. The tube piece adopts S4 shell unit. The shield machine casing adopts S4R shell unit. The grouting layer, soil nail wall surface layer, and pipe trunk main structure adopt C3D8I solid element. The soil nail is made of T3D2 rod unit and embedded in the soil and by the "embeded" command. There are 112,280 physical units in the whole model, with a total of 8640 shell units and 3,560 rod units, totaling 124,520 units and 137,358 nodes. Besides soil nails, the rest of the structure is treated with "Tie." The displacement boundary conditions permitted were no horizontal displacement down the all vertical mesh boundaries, no vertical and horizontal displacement along the bottom boundary of the mesh, and freedom to displace along the top boundary.

4.3. Material Model and Parameters. In the analysis of soil simulation, the compression modulus is selected for the one-dimensional consolidation problem; for the deformation problem, the deformation modulus can be selected [29]. So, for this model, the deformation modulus is selected as one of the soil parameters, and the calculation parameters of the model for selecting a section are shown in Table 3. Among them, ① represents 1-1 artificial fill, ② represents 1-2 plain

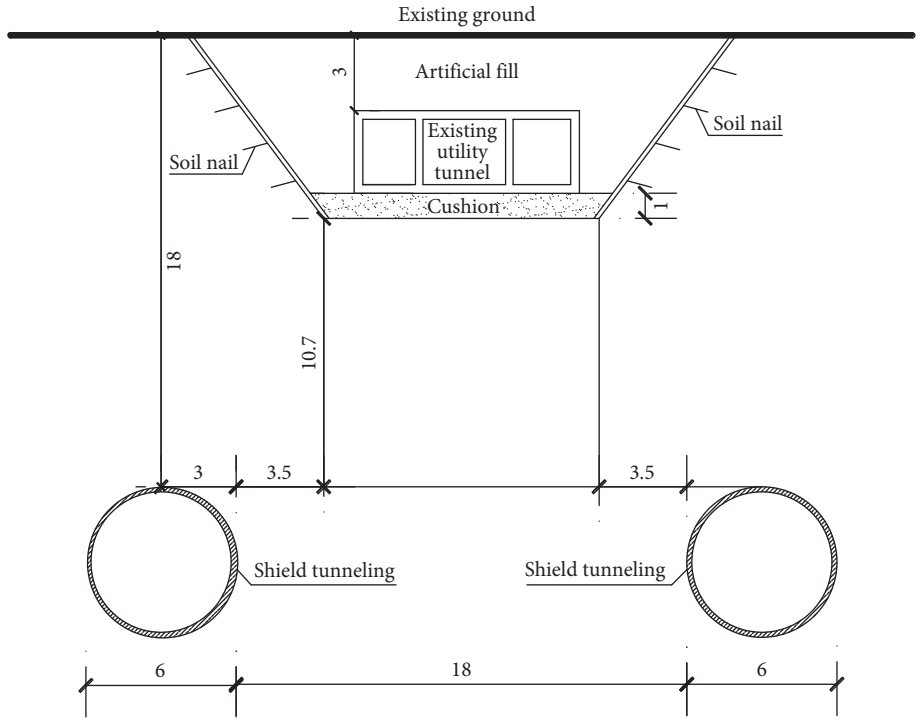

Figure 3: Sketch of relative position of the utility tunnel and metro tunnel (unit: m).

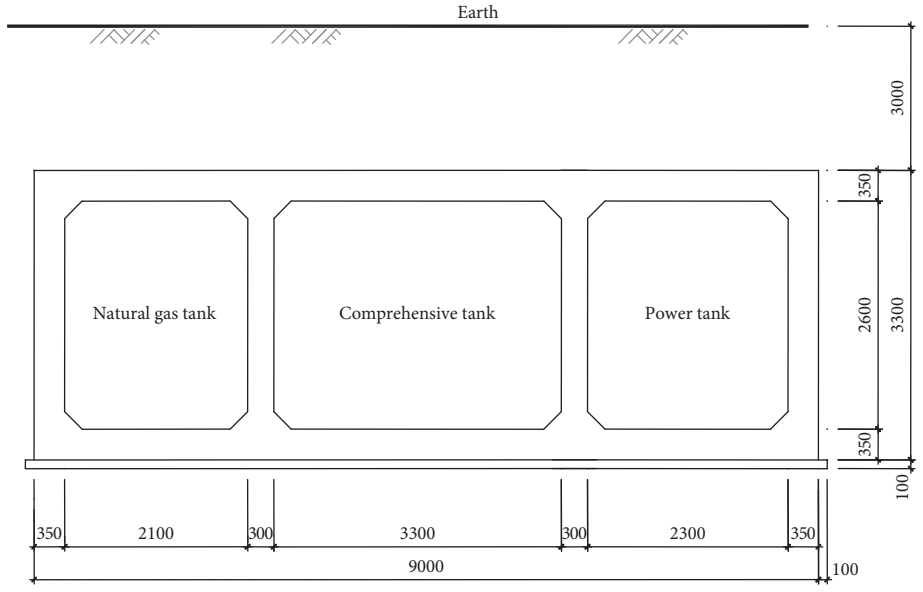

Figure 4: Standard cross-sectional profile of utility tunnel (unit: mm).

fill, ③ represents 3-1-3 new loess, ④ represents 3-2-2 paleosol, and ⑤ represents 4-4 silty clay. The soil constitutive model is selected as follows: ① and ② are linear D-P. ③, ④, and ⑤ are adopted MCC.

The segment of the shield-driven tunnel is C50 reinforced concrete material. Considering the stiffness reduction's effect of the spliced segments, the modulus of elasticity of the segment is reduced by 20%. The elastic modulus of the grouting slurry is corresponding according to the early strength and the late strength taking the value [29–31]. Considering the weight of the entire shield machine, the weight of the shield shell is correspondingly increased in the model, and the structure is simplified to the elastic model. The specific parameters are shown according to the "Code for Design of Concrete Structures" [32] and the "Code for Design of Railway Tunnels" [33] in Table 4.

The soil nail wall modulus of the utility tunnel uses the weighting method, and the corresponding structures of which are simplified to the elastic model. The parameters are selected in accordance with the "Concrete Structure Design

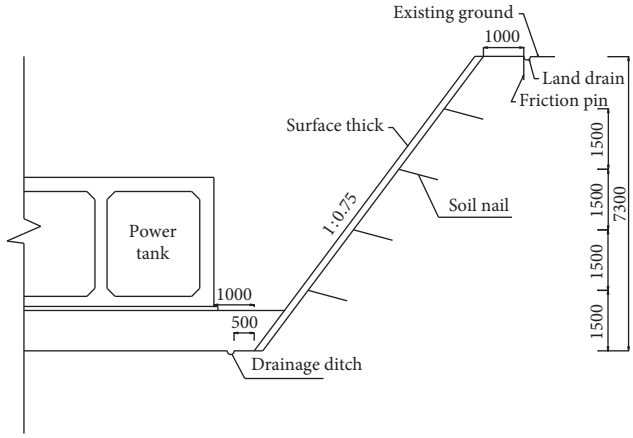

Figure 5: Schematic diagram of the right half of the foundation pit of the pipe gallery (unit: mm).

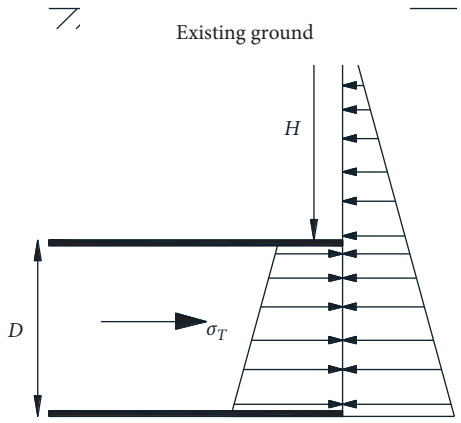

Figure 6: Sketch of support pressure.

Table 2: Calculation table of support pressure.

Condition	Calculation method	Overburden pressure σ_v (kPa)	Top edge support force σ_{top} (kPa)	Lower edge support force σ_{bot} (kPa)
1	All-covering theory	341.700	266.024	354.882
2	The theory of loose earth pressure under the incomplete soil arching effect considering cohesion	218.724	177.481	266.339

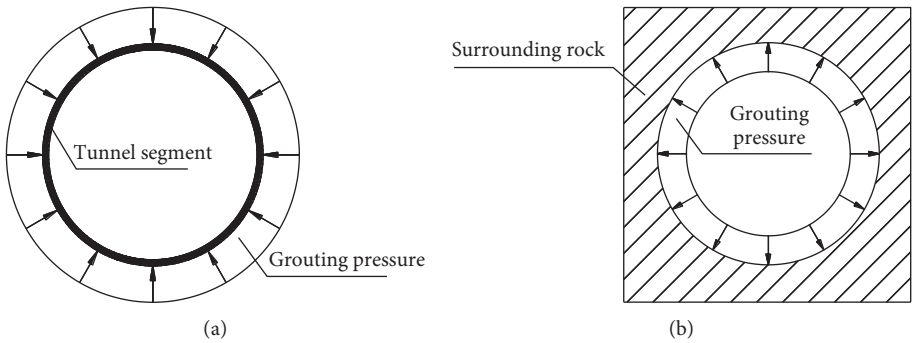

Figure 7: Sketch of synchronous grouting. (a) Segment grouting pressure diagram. (b) Schematic diagram of grouting pressure around the cave.

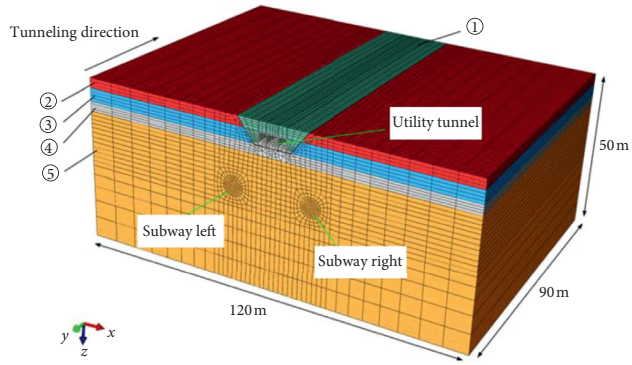

Figure 8: Numerical model of engineering.

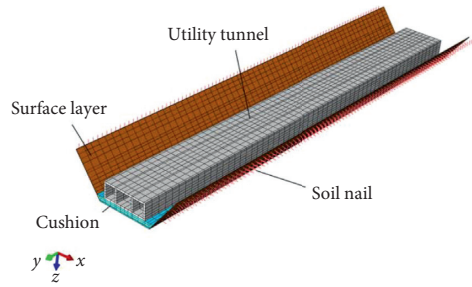

Figure 9: Structures of the foundation pit of the utility tunnel.

Table 3: Soil basic physical property index.

Soil layer	γ (kN/m^3)	E_0 (MPa)	ν	β	d	λ	κ	e_0	M
① 1-1 artificial fill	18.1	4.3	0.28	20.24	30.99	—	—	—	—
② 1-2 plain fill	17	4	0.33	32.94	67.57	—	—	—	—
③ 3-1-3 new loess	18.3	6	0.33	—	—	0.10206	0.00912	0.866	0.77
④ 3-2-2 paleosol	18.9	8	0.31	—	—	0.07687	0.00782	0.756	0.69
⑤ 4-4 silty clay	20.1	13	0.3	—	—	0.06514	0.00782	0.64	0.77

Code" [32] and the "Building Foundation Design Code" [34]. The parameters are shown in Table 5.

4.4. Numerical Simulation Process. The simulation process was divided into two stages: (i) excavation of the existing utility tunnel and (ii) the shield tunneling under the utility tunnel. This paper focuses on the selection of the second stage. After completion of the first stage, the displacement of the soils and structures was reset to zero. Therefore, the calculated uplift values were actually the incremental deformation because of new tunnel excavation.

4.4.1. Construction Course Simulation of the Utility Tunnel. For the excavation of the utility tunnel, according to the principle of no more than 1.5 m and 2.0 m for each excavation and 300 mm from the bottom of the pit, the excavation depth of the foundation pit is arranged as follows.

It is divided into 5 excavations, the first and second excavation depths are 2.0 m, the third and fourth excavation depths are 1.5 m, and the fifth excavation depth is 0.3 m.

In addition, after the excavation, shotcrete with mesh is applied in time and then soil nails are applied. The soil nails are made of HRB400 steel bars with a diameter of 14 mm, a vertical spacing of 1.5 m, and a vertical spacing of 1.0 m. The bedding construction shall be completed immediately after bottoming to minimize the exposure time of the soil at the bottom of the pit. Therefore, the fifth excavation is also bedding construction. Because it is a simulation of the filling during the construction period, the filling process is divided into two simulations here. The specific construction process is as follows:

Step 1: the gravity field is applied to perform the in situ ground stress balance, and the displacement increment is controlled to be on the order of e^{-4} degree. The principle of this step is nonlinear iteration. Iteration may be used to ensure that equilibrium is achieved at each step of the analysis to within a specified convergence tolerance. Through repeated iterations to correct the solution results until convergence, it has a better convergence effect. The iterative method in Abaqus uses the tangent stiffness iteration method. The

Table 4: Parameters of structures of metro tunnel.

Subject	γ (kN/m^3)	E (MPa)	ν	Layer (m)
Shield	463.84	$2.10E+05$	0.30	0.04
Segment	25	$2.84E+04$	0.20	0.3
Grouting (early)	23	0.9	0.30	—
Grouting (late)	23	400	0.2	—

"—" means that the grouting layer completely fills the gap at the shield tail, without a fixed thickness.

Table 5: Parameters of structures of the utility tunnel.

Subject	γ (kN/m^3)	E (MPa)	ν
Soil-nailed wall	22	$2.18E+04$	0.2
Soil nailing	78.5	$2.00E+05$	0.3
Cushion	23	$2.60E+04$	0.2
Corridor	25	$3.15E+04$	0.2

tangent stiffness iterative method is a variable stiffness iterative method, which uses changing tangent stiffness to continuously modify the iterative result. This method is also called the Newton–Raphson method, which has high iteration accuracy.

Step 2: for the first excavation, it uses the "Model Change" command that comes with ABAQUS to invalidate excavation soil (within 2.0 m depth) and activates soil nails and surface units within 2.0 m depth.

Step 3: the second, third, and fourth excavations are consistent with what was done in Step 2.

Step 4: in the fifth excavation, it uses the "Model Change" command that comes with ABAQUS to invalidate the fifth layer (0.3 m thick) of soil and activates the surface layer and cushion unit.

Step 5: it constructs the pipe gallery and then activates the pipe gallery unit.

Step 6: for the first backfill, filling at the same elevation at the top of the pipe gallery will activate the backfill soil unit in the corresponding range.

Step 7: for the second backfill, it fills back to the design height (the surface) and activates the backfill soil within the corresponding range.

4.4.2. Construction Course Simulation of the Shield-Driven Tunnel. The length of the TBM shield machine is set to be 9 m, which is equal to the width of 6 rings. In the first stage, elaborate simulation of the shield tunneling process was conducted, and the simulation steps are as follows (the drifting footage is 1.5 m, which is equal to width of 1 ring):

Step 1: the gravity field is applied to perform the in situ ground stress balance, and the displacement increment is controlled to be on the order of e^{-4} degree.

Step 2: using the "Model Change" command that comes with ABAQUS to invalidate excavation soil of the left tunnel (LT), the construction advances the first ring. At the same time, the pressure acting is applied on the tunnel face top to activate the first ring of the shield shell.

Step 3: the second step is to be recycled until the 7th ring is excavated. At the same time as the failure treatment of the excavated soil, the tail unit of the shield machine casing is also failed. At this time, it keeps the length of the shield machine unchanged (6 rings) and activates segment unit of the LT and the jet grouting unit, at which time the strength of the jet grouting is the early strength and the grouting pressure is applied.

Step 4: the second and third steps are to be recycled until the 13th ring is excavated. At this time, on the basis of the first two steps, the grouting pressure at the tail of the segment is invalidated, and the strength of the jet grouting is adjusted to the late strength.

Step 5: the third and fourth steps are to be recycled. It keeps the length of the shield shell of the shield machine to 6 rings (the length of the shield machine). The jet grouting range is within the 6-ring piece until the tunneling of the shield machine is completed.

Step 6: the construction process of the right tunnel (RT) can be repeated in the above Steps 2 and 5.

4.5. Arrangement of Monitoring Points and Time of the Utility Tunnel. The monitoring lines are arranged inside the three cabins of the utility tunnel. Here, for the convenience of description, the natural gas tank is briefly described as the left cabin (LC), the comprehensive tank is briefly described as the middle cabin (MC), and the power tank is briefly described as the right cabin (RC). Along the pipe gallery axis, monitoring lines are arranged on the roof and floor of the three cabins, namely, the LC floor survey line LBC-1, the LC roof survey line LCT-4, the MC floor survey line MCB-2, the MC roof survey line MCT-5, the RC floor line RCB-3, and the RC roof line RCT-6.

Since the model is symmetrical in the longitudinal direction, the middle section of the pipe gallery is selected as the monitoring section. That is, the position corresponding to the 30th ring (at 45 m) of the tunnel segment. The monitoring lines are set on the top and bottom sections of the section as R30-7 and R30-8. The specific layout diagram is shown in Figure 10.

In addition, monitoring points are laid at the midpoint of each cabin of the monitoring section of the pipe gallery as shown in Figure 11. The midpoint of the midcabin here refers to the point where the midpoint between the two tunnels is projected to the pipe gallery.

It selects the typical monitoring time as the left line advances to 15th, 30th, and 45th rings and the right line advances to 15th, 30th, and 45th rings. That is, the heading face of the shield machine reaches 15 rings in front of the monitoring sections, directly below the monitoring section, and 15 rings away from the monitoring section. The relative positional relationship between the shield machine and the pipe gallery at the time of monitoring is shown in Figure 12.

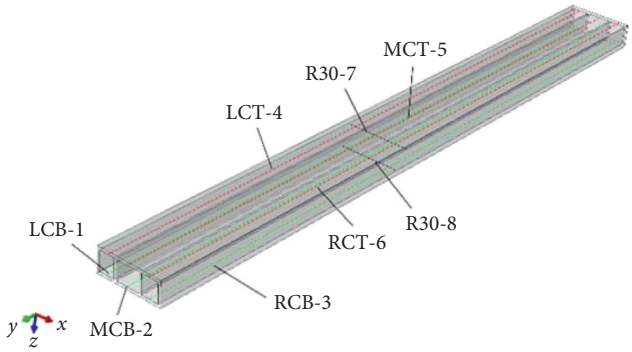

Figure 10: Monitoring line arrangement in the utility tunnel.

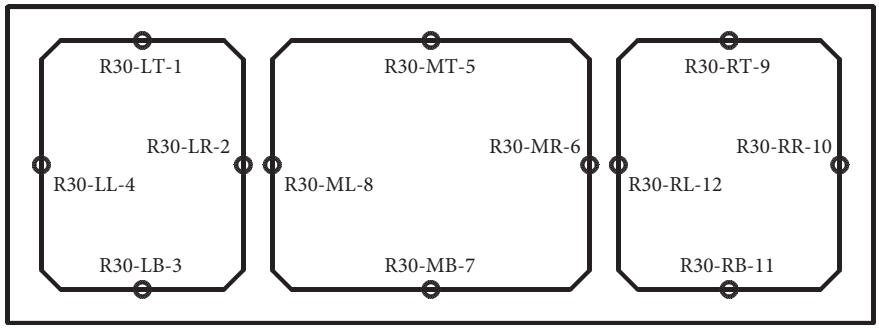

Figure 11: Monitoring points arrangement on cross section of the utility tunnel.

5. Deformation Behaviors of the Existing Utility Tunnel

The urban underground common trench is a shelter for multiple underground pipelines, and its deformation control standards should be stricter than the general pipeline. However, at this stage, the relevant regulations for the utility tunnel in China are not yet complete. The relevant deformation standard of the underground pipeline of degree 1 level of magnitude of pipelines is the benchmark; that is, the maximum settlement value is −10 mm. In addition, for the uplifting, this article is selected according to the subway control standards, that is, the maximum value of the uplifting is 5 mm.

5.1. Analysis of Vertical Displacement of Pipe Gallery Cross-Sectional Monitoring Point. During the whole shield tunnel construction process, the vertical displacement of the monitoring points arranged on the monitoring section is shown in Figure 13.

It can be observed in Figure 13 that the displacement law of the top and bottom plate measuring points is the same and the displacement law of the monitoring points on both sides of the pipe gallery partition wall is similar. From the settlement value of each measuring point, the final settlement of R30-LL-4 is the largest at −3.18 mm, and the settlement of R30-RR-10 is the smallest at −1.74 mm. At the same time, it can be found that the closer the monitoring point to the construction side, the earlier the settlement occurs. After the completion of the construction, the vertical displacement of each measurement point is shown as a settlement.

According to the curve in the figure, it can be found that with the midcabin monitoring point (R30-MT-5 and R30-MB-7) as the center of symmetry, the displacement laws of the monitoring points on the left and right sides are different. To simplify the difficulty of analysis, only two typical points were selected for analysis, which were R30-LL-4 near the left line and R30-RR-10 near the right line.

During the construction on the left line, during the first few rounds of construction, the uplift phenomenon would appear at both measuring points. The uplift value of R30-LL-4 was relatively small, while that of R30-RR-10 was relatively large. With the advancement of the shield machine, it can be found that the vertical displacement curves of the two measuring points are different. The performance is that R30-LL-4 begins to sink, and the uplift value of R30-RR-10 gradually increases. The peak of the uplift was 0.38 mm during the excavation of the 19th ring (the first uplift). After the 19th ring, R30-RR-10 began to appear to settle. At this time, R30-LL-4 still maintained the trend of settlement until the construction of the 41st ring. The settlement of R30-RR-10 reached a peak of 0.22 mm. After the 41st ring, R30-LL-4 still maintained the trend of subsidence, and R30-RR-10 bulged again (the second bulge). After the completion of the construction of ring 60, the uplift stopped. The settlement of R30-LL-4 reached the peak value of −3.83 mm, and the peak value of the second uplift of R30-RR-10 was 0.6 mm. In the

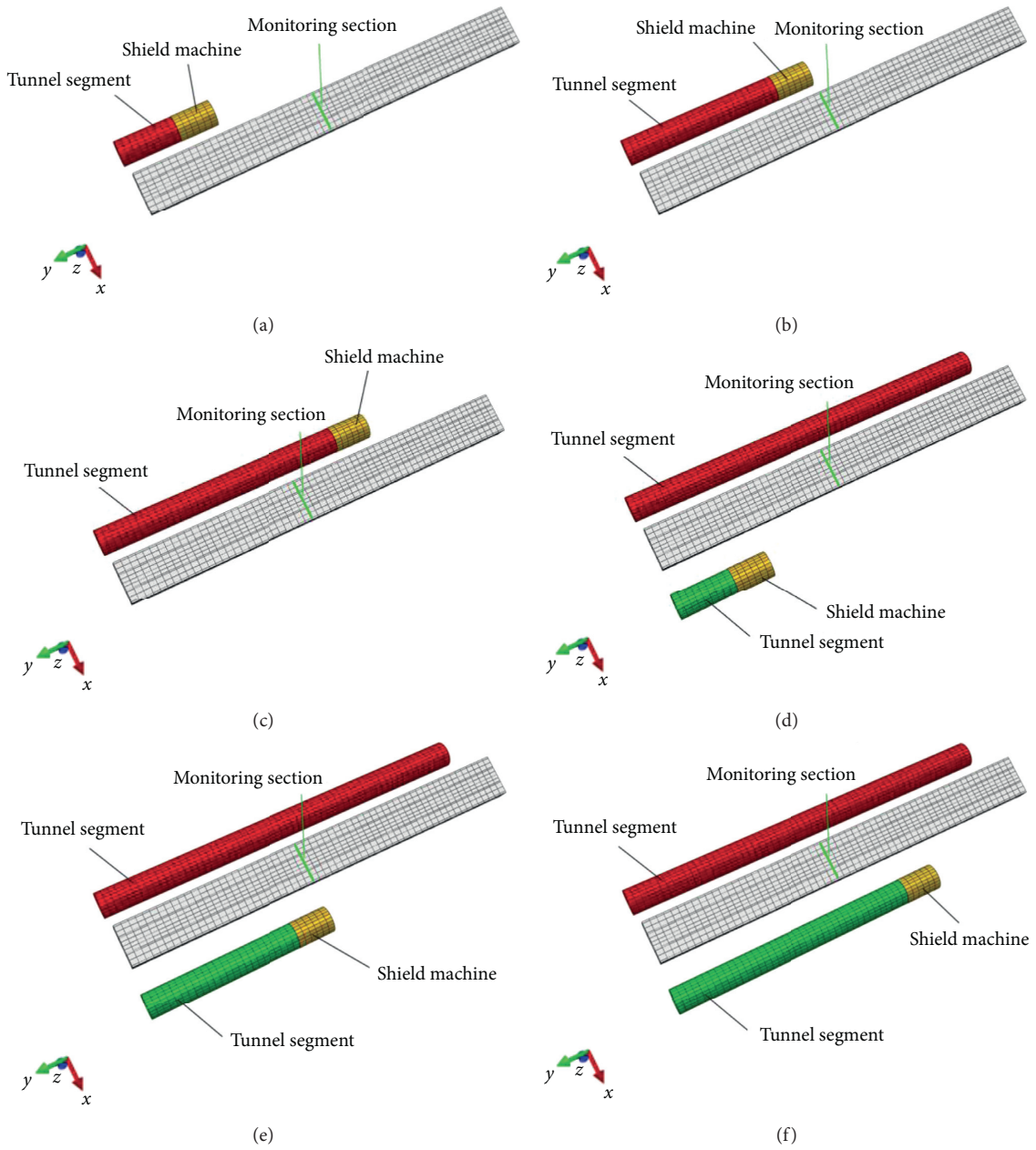

Figure 12: Relative position of the shield machine and utility tunnel at the selected moment of monitoring. (a) Left lane to 15th ring. (b) Left lane to 30th ring. (c) Left lane to 45th ring. (d) Right lane to 15th ring. (e) Right lane to 30th ring. (f) Right lane to 45th ring.

subsequent construction progress, the two monitoring points remained relatively stable until the construction of the left line was completed.

During the excavation of the right line, the two measuring points will be uplifted during the first few loops of construction. For now, the measuring point R30-RR-10 becomes the point near the construction side, and the measuring point R30-LL-4 becomes a point far away from the construction side. The measurement point R30-RR-10 will maintain settlement, while the measurement point R30-LL-4 is the phenomenon of R30-RR-10 during the construction of the left line. Due to the secondary construction disturbance and when completed, the final settlement value of R30-LL-4 (−3.18 mm) will be less than the maximum settlement value (−3.83 mm). The measuring point R30-RR-10 will eventually settle instead of uplifting, and its final settlement will be −1.74 mm.

5.2. Comparison of Vertical Displacement of Pipeline Axial Survey Line. Because the vertical displacement of the top and bottom of the pipe gallery is consistent with the vertical displacement law, the axial survey line at the bottom of the pipe gallery under two conditions is selected for analysis.

The more typical monitoring time is the left line advancing 30 circles and the right line advancing 30 rings. The

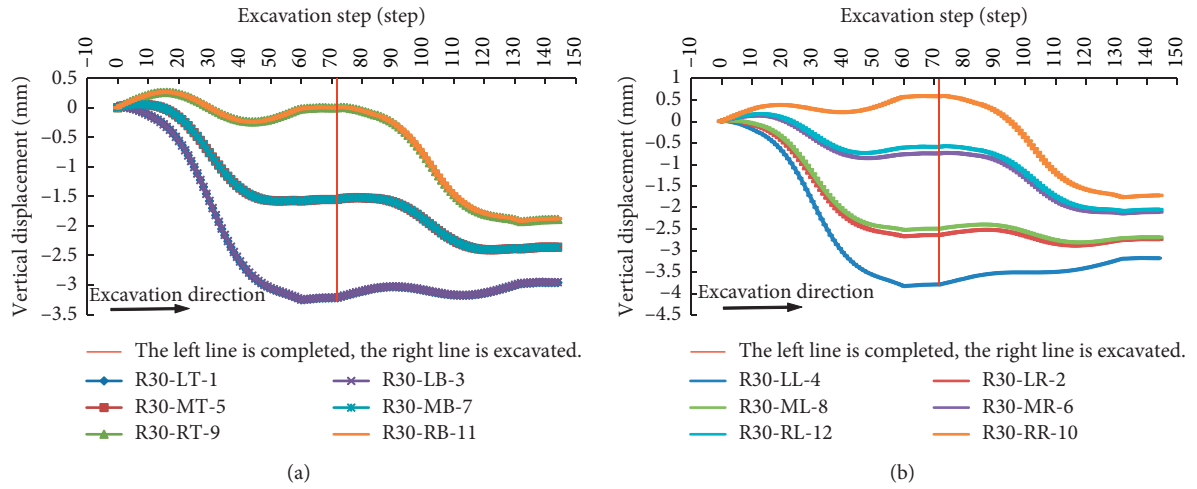

Figure 13: The vertical displacement curves of each monitoring point during construction: (a) pipe gallery top and bottom; (b) pipe gallery wall.

vertical displacement of each longitudinal survey line is shown in Figure 14.

Because the support pressure is reduced by considering the soil arch effect in condition 2, a large settlement in front of the palm face is expected, which is consistent with the phenomenon shown in the data in Figure 14.

For line LCB-1, during the construction of left line (Figure 14(a)), the starting point of working condition 1 in front of the palm face is earlier than that of working condition 2, and the horizontal distance between them is about 2D. In addition, due to the small support pressure in working condition 2, the settlement in front of the palm face is slightly larger than that in working condition 1, and the difference between the two settlements is smaller. In the subsequent settlement after the shield machine passes, the settlement value of the working condition 2 is smaller than that of the working condition 1, and the difference is also small. At the same time, it can be found that the settlement of the two working conditions is basically the same within the length of the shield machine behind the palm face. During the construction of the right line (Figure 14(b)), the location rule of the settlement point in front of the palm face is consistent with that of the left line, but the difference between the two in vertical displacement value is obvious. The settlement is significantly larger than that of working condition 1. Within the length of the shield machine behind the palm face, the vertical displacement curve of working condition 2 is smoother than that of working condition 1. Similarly, the settlement value of working condition 2 is greater than the working condition 1 after the shield machine is slightly smaller, and the difference between the two is not large.

For line MCB-2, during the construction of left line (Figure 14(c)), the starting point of working condition 1 in front of the same palm face is closer than that of working condition 2. The horizontal distance between the two starting points is about 0.5 d, and the settlement difference is not large. The settlement rule of the two working conditions within the length of the shield machine is basically the same. Beyond the shield machine, the settlement of working condition 2 is smaller than that of working condition 1, and the settlement difference between the two working conditions is not large. During the construction on the right line (Figure 14(d)), the settlements in the front of the palm face are significantly different. The settlement in working condition 2 is larger than that in working condition 1. Within the range of the length of the shield machine, the settlement is relatively gentle in working condition 2.

For line RCB-3, during the construction of the left line (Figure 14(e)), the vertical displacement in front of the palm face in both cases shows a bulging phenomenon. The uplift difference in working condition 2 is smaller than that in working condition 1, and the rest of the rules are basically the same as the above two lines.

In conclusion, during the left line construction, there is no significant difference in the effect of controlling the vertical displacement of the pipe gallery in the working condition 1 and condition 2 with less support pressure. During the right line construction, the control effect in the working condition 2 is not as obvious as that in the working condition 1. The main difference is that the settlement in front of the palm surface in the working condition 2 is larger than that in the working condition 1.

5.3. Comparison of Vertical Displacement of Monitoring Points in the Cross Section of the Pipe Gallery. This section selects the representative monitoring points R30-LL-4 that is closest to the left line and R30-RR-10 that is closest to the right line in the monitoring section for comparison and analysis, as shown in Figure 15.

During the entire construction process in Figure 15, the variation of vertical displacement of the two working conditions of monitoring points is consistent. The settlement value of working condition 2 is larger than that of working condition 1. It is −4.0 mm at the measuring point R30-LL-4.

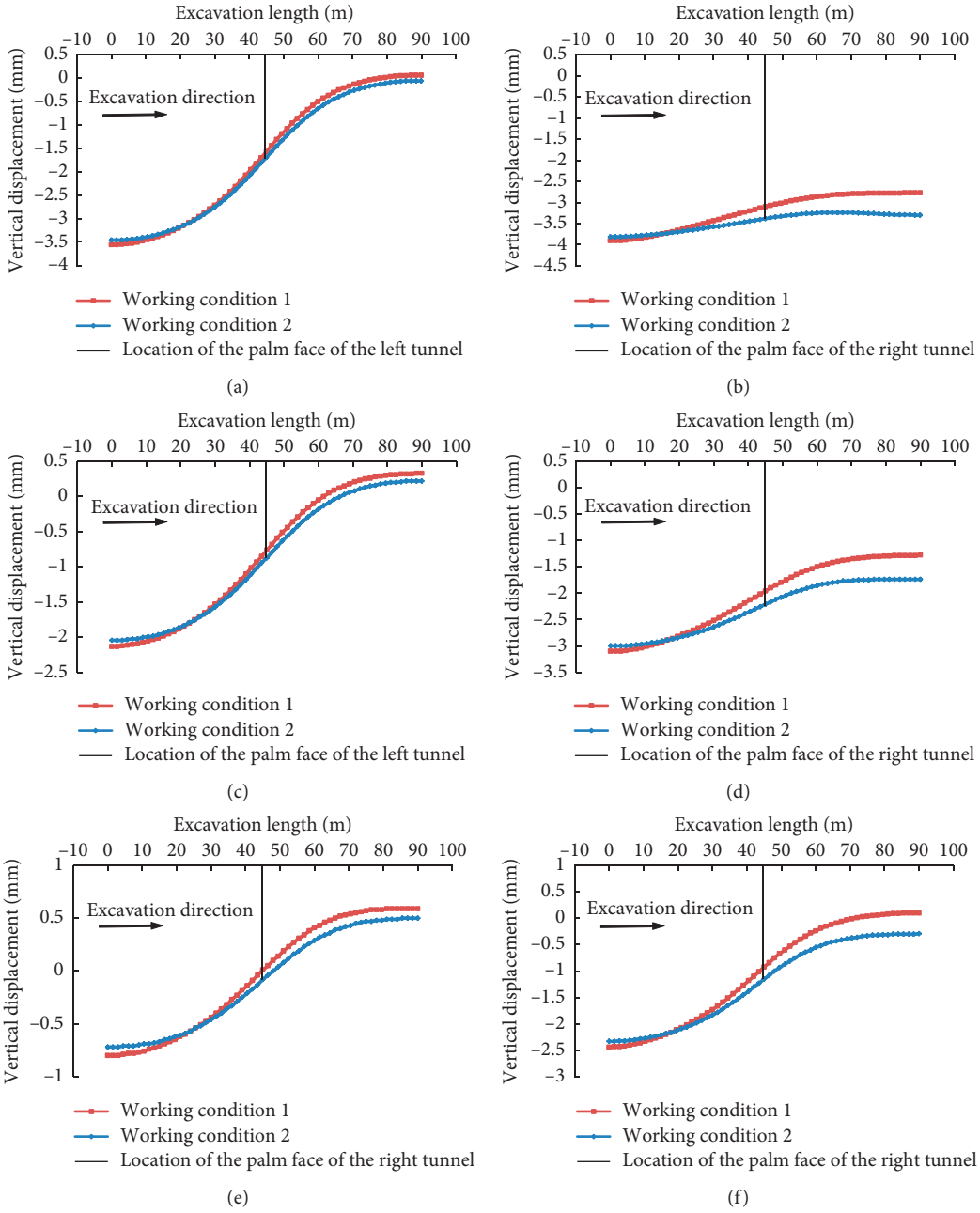

Figure 14: The vertical displacement curves of each monitoring longitudinal line in two cases at the selected moment. (a) Vertical displacement of LCB-1 when the left line is advanced to 30 rings. (b) Vertical displacement of LCB-1 when the left line is advanced to 30 rings. (c) Vertical displacement of MCB-2 when the left line is advanced to 30 rings. (d) Vertical displacement of MCB-2 when the left line is advanced to 30 rings. (e) Vertical displacement of RCB-3 when the left line is advanced to 30 rings. (f) Vertical displacement of RCB-3 when the left line is advanced to 30 rings.

The uplift value of the working condition 1 is larger than the working condition 2. It is 0.6 mm at the measuring point R30-RR-10. In addition, the vertical displacement difference between the two conditions during the left line construction is not large, and the vertical displacement difference will increase during the right line construction.

In summary, under the condition that the remaining conditions remain unchanged, due to the consideration of the soil arch effect in case 2, the settlement value is large and the uplift value is small. That is to say, the trend of lateral up warping decreases with the decrease of support pressure. For the construction method of "completion of the left line,

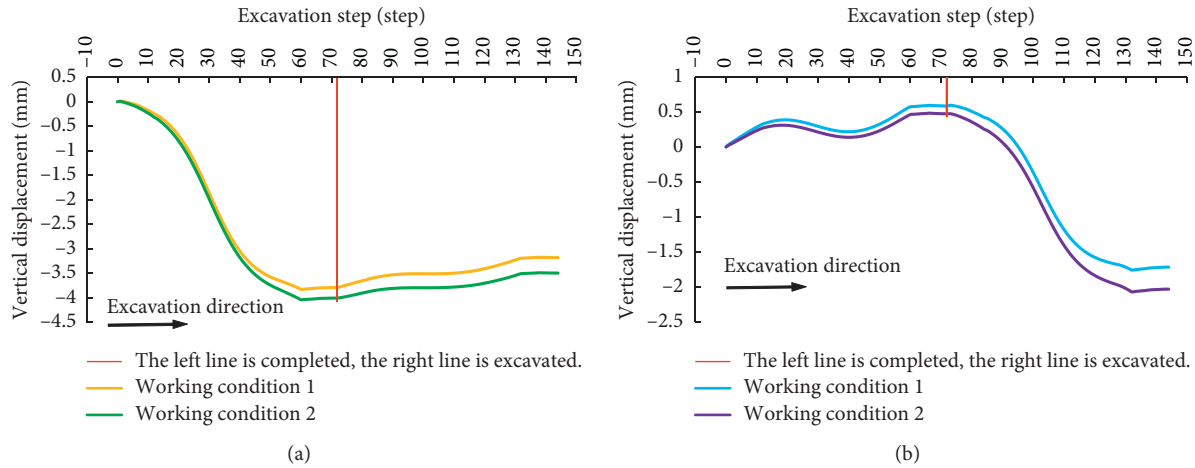

Figure 15: The vertical displacement curves of monitoring points (a) R30-LL-4 and (b) R30-RR-10 during construction.

reexcavation of the right line," under the reasonable support pressure value theory, this paper considers that the influence of vertical displacement of the pipe gallery caused by different support pressures is mainly reflected in the process of excavation of the back line.

For the working condition 2 in which the soil arch effect is considered, the maximum settlement is −4.0 mm and the maximum uplift is 0.48 mm. Both the settlement and the uplift do not exceed the displacement control standards. Therefore, under the condition of spatial layout of underground buildings in this paper, considering the soil arch effect, the construction of the metro shield tunnel will not have a destructive impact on the existing comprehensive pipe gallery, which is safe.

6. Conclusions

This paper investigates the stability influence of twin tunnels excavation under the existing pipe gallery tunnel. Based on the calculated results, the following conclusions can be drawn:

(1) Loess is a special kind of clayed soil. In the theoretical calculation of overburden earth pressure of shield tunnel in Xi'an loess, the loose earth pressure theory under the incomplete soil arching effect can be used for calculation when considering the soil arching effect.

(2) In the case where the left and right lines are constructed at different times, the vertical displacement of the pipe gallery is affected by different support pressures. If the support pressure is small, the settlement will be large, and the uplift will be small. That is to say, the overall deformation of the pipe corridor is mainly subsidence, and the lateral upturning does not increase with the increase in settlement on the side of the pipe gallery settlement.

(3) In this paper, under the combined conditions of underground comprehensive pipe corridor and subway line, it is applicable to the supporting pressure calculated by different overlying earth pressure theories. According to the construction method and supporting pressure of this article, shield tunnel construction will not affect the safety of the comprehensive pipe corridor.

Data Availability

All data used in this study are available from the corresponding author upon request. This paper uses ABAQUS finite element software to build a three-dimensional model and for calculation.

Conflicts of Interest

The authors declare that they have no conflicts of interest.

Acknowledgments

This research was financially supported by the Xi'an University of Technology Foundation (107/256211404), Loess Soil Mechanics and Engineering Key Laboratory of Shaanxi Province Foundation (13JS073), Natural Science Foundation of Shaanxi Province (2017JM5059), and National Natural Science Foundation of China (Grant Nos. 11572246 and 51779207).

References

[1] R. P. Chen, J. Zhu, W. Liu, and X. W. Tang, "Ground movement induced by parallel EPB tunnels in silty soils," *Tunnelling and Underground Space Technology*, vol. 1, no. 26, pp. 163–171, 2011.

[2] R. P. Chen, L. J. Tang, D. S. Ling, Y. M. Chen, and Y. M. Chen, "Face stability analysis of shallow shield tunnels in dry sandy ground using the discrete element method," *Computers and Geotechnics*, vol. 38, no. 2, pp. 187–195, 2011.

[3] S. Ma, Y. Shao, Y. Liu, J. Jiang, and X. Fan, "Responses of pipeline to side-by-side twin tunnelling at different depths: 3D centrifuge tests and numerical modelling," *Tunnelling and Underground Space Technology*, vol. 66, pp. 157–173, 2017.

[4] R.-p. Chen, J. Li, L.-g. Kong, and L.-j. Tang, "Experimental study on face instability of shield tunnel in sand," *Tunnelling and Underground Space Technology*, vol. 33, pp. 12–21, 2013.

[5] R. Chen, X. Yin, L. Tang, and Y. Chen, "Centrifugal model tests on face failure of earth pressure balance shield induced by steady state seepage in saturated sandy silt ground," *Tunnelling and Underground Space Technology*, vol. 81, no. 81, pp. 315–325, 2018.

[6] K. Soga, R. G. Laver, and Z. Li, "Long-term tunnel behaviour and ground movements after tunnelling in clayey soils," *Underground Space*, vol. 2, no. 3, pp. 149–167, 2017.

[7] R. E. Ranken and J. Ghaboussi, "Analysis of interaction between two parallel tunnels," *Finite Element Method*, vol. 34, no. 2, pp. 45–52, 1976.

[8] V. Avgerinos, D. M. Potts, and J. R. Standing, "Numerical investigation of the effects of tunnelling on existing tunnels," *Geotechnique*, vol. 67, no. 9, 2017.

[9] C. W. W. Ng, K. Y. Fong, and H. L. Liu, "The effects of existing horseshoe-shaped tunnel sizes on circular crossing tunnel interactions: three-dimensional numerical analyses," *Tunnelling and Underground Space Technology*, vol. 77, pp. 68–79, 2018.

[10] M. Yin, H. Jiang, Y. Jiang, Z. Sun, and Q. Wu, "Effect of the excavation clearance of an under-crossing shield tunnel on existing shield tunnels," *Tunnelling and Underground Space Technology*, vol. 78, pp. 245–258, 2018.

[11] Z. Zhang and M. Huang, "Geotechnical influence on existing subway tunnels induced by multiline tunneling in Shanghai soft soil," *Computers and Geotechnics*, vol. 56, pp. 121–132, 2014.

[12] M. Maleki, H. Sereshteh, M. Mousivand, and M. Bayat, "An equivalent beam model for the analysis of tunnel-building interaction," *Tunneling and Underground Space Technology*, vol. 26, no. 9, pp. 524–533, 2011.

[13] J. Liu, T. Qi, and Z. Wu, "Analysis of ground movement due to metro station driven with enlarging shield tunnels under building and its parameters sensitivity analysis," *Tunneling and Underground Space Technology*, vol. 28, no. 8, pp. 287–296, 2012.

[14] P. B. Attewell, J. Yeates, and A. R. Selby, *Soil Movements Induced by Tunnelling and Their Effects on Pipelines and Structures*, Blackie & Son, London, UK, 1986.

[15] A. Klar, T. E. B. Vorster, K. Soga, and R. J. Mair, "Soil-pipe interaction due to tunnelling: comparison between Winkler and elastic continuum solutions," *Géotechnique*, vol. 55, no. 6, pp. 461–466, 2005.

[16] A. Klar, T. E. Vorster, K. Soga, and R. J. Mair, "Elastoplastic solution for soil-pipe-tunnel interaction," *Journal of Geotechnical and Geoenvironmental Engineering*, vol. 133, no. 7, pp. 782–792, 2007.

[17] A. Klar and A. M. Marshall, "Linear elastic tunnel pipeline interaction: the existence and consequence of volume loss equality," *Géotechnique*, vol. 65, no. 9, pp. 788–792, 2015.

[18] T. E. Vorster, A. Klar, K. Soga, and R. J. Mair, "Estimating the effects of tunneling on existing pipelines," *Journal of Geotechnical and Geoenvironmental Engineering*, vol. 131, no. 11, pp. 1399–1410, 2005.

[19] Y. Wang, Q. Wang, and K. Y. Zhang, "An analytical model for pipe-soil-tunneling interaction," *Procedia Engineering*, vol. 14, pp. 3127–3135, 2011.

[20] C. Lin, M. Huang, F. Nadim, and Z. Liu, "Tunnelling-induced response of buried pipelines and their effects on ground settlements," *Tunnelling and Underground Space Technology*, vol. 96, pp. 103–193, 2020.

[21] K. Terzaghi, "Stress distribution in dry and in saturated sand above a yielding trap-door," in *Proceedings of First International Conference on Soil Mechanics and Foundation Engineering*, pp. 307–311, Cambridge, MA, USA, June 1936.

[22] R. L. Handy, "The arch in soil arching," *Journal of Geotechnical Engineering*, vol. 111, no. 3, pp. 302–318, 1985.

[23] C. Li, "Method for calculating loosening earth pressure during construction of shield tunnels," *Chinese Journal of Geotechnical Engineering*, vol. 36, no. 9, pp. 1714–1720, 2014.

[24] N. Loganathan and H. G. Poulos, "Analytical prediction for tunneling-induced ground movements in clays," *Journal of Geotechnical and Geoenvironmental Engineering*, vol. 124, no. 9, pp. 846–856, 1998.

[25] C. Zhu, *Research on Ground Settlements Induced by Subway Shield Tunnel Construction in Xi'an Loess Strata*, Xi'an University of Technology, Xi'an, China, 2009.

[26] C. Ou, *Deep Excavation Theory and practice*, Taylor and Francis Group, London, UK, 2006.

[27] Z. Zhang and W. Hu, "Investigation on excavation face support pressure calculation methods of shield tunnelling in clayey soil," *Chinese Journal of Rock Mechanics and Engineering*, vol. 33, no. 3, pp. 606–614, 2014.

[28] F. Ye, C. Gou, J. Mao, P. Yang, Z. Chen, and T. Jia, "Calculation of critical grouting pressure during shield tunneling in clay stratum and analysis of the influencing factors," *Rock and Soil Mechanics*, vol. 36, no. 4, pp. 937–945, 2015.

[29] L. Wang, *Study on Interaction Mechanism and Deformation Control Standard of Collapsible Loess Layer and Metro Structure*, Chang'an University, Xi'an, China, 2016.

[30] C. Zhu, Li Ning, H. Liu, and Z. Zhang, "Analysis of ground settlement induced by workmanship of shield tunnelling," *Rock and Soil Mechanics*, vol. 32, no. 1, pp. 158–164, 2011.

[31] C. Zhu, Li Ning, and Z. Zhang, "Analysis and prediction of ground settlement induced by shield construction in Xi'an loess strata," *Chinese Journal of Geotechnical Engineering*, vol. 32, no. 7, pp. 1087–1095, 2010.

[32] GB50010-2010, *Ministry of Housing and Urban-Rural Development of the People's Republic of China. GB50010-2010 Code for Design of Concrete structures*, China Architecture and Building Press, Beijing, China, 2015, in Chinese.

[33] TB10003-2016, *National Railway Administration of the People's Republic of China. TB10003-2016 Code for Design of Railway tunnel*, China Railway Press, Beijing, China, 2016, in Chinese.

[34] GB50007-2011, *Ministry of Housing and Urban-Rural Development of the People's Republic of China. GB50007-2011 Code for Design of Building Foundation*, China Architecture and Building Press, Beijing, China, 2011, in Chinese.